Journal of Materials Chemistry B

ROYAL SOCIETY OF CHEMISTRY

PAPER

View Article Online
View Journal | View Issue

Check for updates

Cite this: J. Mater. Chem. B, 2025, 13, 12172

Enhanced mRNA and pDNA delivery *via* PEGylated solid lipid nanoparticles with an optimally balanced ionizable/cationic lipid content

Nipuni Maniyamgama,[ab] Ki Hyun Bae,[a] Jialing Lee,[a] James Hoi Po Hui[b] and Yi Yan Yang *[ab]

Received 3rd March 2025,
Accepted 30th July 2025

DOI: 10.1039/d5tb00470e

rsc.li/materials-b

Non-viral gene delivery holds significant promise for the treatment of various diseases. Solid lipid nanoparticles (SLNs) are emerging as promising gene delivery vehicles due to their ease of manufacture and high stability. However, the development of efficient and safe SLNs remains a challenge. This study aims to develop ionizable lipid-incorporated PEGylated SLNs (PEG-iSLNs) for effective mRNA and plasmid DNA (pDNA) delivery. Using a solvent emulsification/evaporation technique, a series of PEG-iSLNs were formulated at various weight ratios of the ionizable lipid ALC-0315 to the cationic lipid DOTMA. PEG-iSLNs formulated at an optimal ALC-0315/DOTMA ratio had superior mRNA transfection potency and membrane fusion activity over those with either ALC-0315 or DOTMA alone. iSLNs and PEG-iSLNs appeared to remain stable during storage at 4 °C over 18 and 12 months, respectively. Bioluminescence imaging study demonstrated the feasibility of the top-performing candidate, PEG-iSLN-3, for *in vivo* delivery of mRNA *via* both intramuscular and footpad subcutaneous routes, highlighting its potential as an efficient and nontoxic delivery vehicle for diverse nucleic acid cargoes.

Introduction

Lipid nanoparticles (LNPs) have recently emerged as promising vehicles for delivery of nucleic acid therapeutics. Patisiran, a LNP-based formulation of transthyretin-targeted siRNA, has been proven efficacious for the treatment of hereditary transthyretin-mediated amyloidosis.[1] Additionally, LNPs have played a crucial role in the success of two COVID-19 mRNA vaccines (BNT162b2 and mRNA-1273).[2] LNPs are primarily composed of 4 lipid components: an ionizable lipid bearing a tertiary amine head group, a helper phospholipid, cholesterol and a polyethylene glycol (PEG)-lipid conjugate. Among them, the ionizable lipid (*e.g.*, ALC-0315 and SM-102 used in the BNT162b2 and mRNA-1273 formulations, respectively) has been considered a key component of LNP-based nucleic acid delivery systems. For example, the ionizable lipid is designed to have a near-neutral charge at extracellular fluid pH (~7.4), thus reducing LNP-associated toxicity. Moreover, the tertiary amine group of ionizable lipids becomes protonated at endosomal pH (5.5–6.5) and associates with anionic endosomal phospholipids, thereby facilitating the membrane fusion and favoring delivery of the nucleic acid payload into the cytoplasm of target cells.[3,4]

Solid lipid nanoparticles (SLNs) are colloidal nanocarriers having a solid lipid core stabilized by an amphiphilic lipid shell layer. Recently, SLNs have gained increasing attention as nucleic acid delivery vectors due to their ease of manufacture, high colloidal stability and improved bioavailability.[5] Most prior studies have focused on the use of cationic lipid-modified SLNs to condense nucleic acid payloads into nano-sized complexes with a positive surface charge, which can readily cross the negatively charged cell membranes *via* adsorptive endocytosis.[6,7] However, the introduction of permanently positive-charged lipids has been reported to cause cellular toxicity, blood platelet activation and inflammation *in vivo*.[8–10] In addition, the strong binding between cationic SLNs and anionic nucleic acid molecules can negatively affect transfection efficiency due to insufficient dissociation after cellular uptake.[11] Therefore, it is highly desirable to explore alternative approaches to improve the transfection efficiency of SLNs while mitigating their toxicity.

Herein, we report the development of ionizable lipid-incorporated SLNs (iSLNs) as efficient and non-toxic carriers for nucleic acid delivery. We hypothesize that mixing an ionizable lipid with a cationic lipid at an optimal ratio would allow for adjustment of the apparent acid dissociation constant (pK_a)

[a] Bioprocessing Technology Institute (BTI), Agency for Science, Technology and Research (A*STAR), 20 Biopolis Way, Centros #06-01, Singapore 138668, Republic of Singapore. E-mail: yyyang@bti.a-star.edu.sg
[b] Department of Orthopaedic Surgery, Yong Loo Lin School of Medicine, National University of Singapore, 21 Lower Kent Ridge Road, Singapore 119077, Republic of Singapore

of iSLNs within the early endosomal pH range (5.5–6.5).[12] These iSLN formulations are anticipated to acquire a more positively charged surface as the endosomal pH drops below the pK_a, facilitating their entry to the cytoplasm by disrupting the endosomal membrane. At cytosolic pH (7.2–7.4), the electrostatic interactions between iSLNs and nucleic acids would weaken as the surface charge of iSLN decreases, ultimately promoting the complex dissociation and cargo release.[13] To verify our hypothesis, we developed a series of iSLN formulations by combining the ionizable lipid ALC-0315 with the cationic lipid DOTMA at different weight ratios and evaluated their applicability for delivery of mRNA and pDNA. Interestingly, iSLN-3 and its PEGylated counterpart (PEG-iSLN-3) formulated at an ALC-0315/DOTMA ratio of 2 : 2 exhibited superior mRNA/pDNA transfection efficiency over those with either ALC-0315 or DOTMA alone *in vitro*. Mechanistic studies revealed that PEG-iSLN-3 was more efficient in escaping the endosomes than the benchmark ALC-LNP *via* the enhanced membrane-disruptive activity. *In vivo* mRNA delivery efficacy of PEG-iSLN-3 was validated in BALB/c mice using two common routes of vaccination: intramuscular and footpad subcutaneous administration. These findings suggest the potential utility of PEG-iSLN-3 as a mRNA delivery system for prophylactic applications.

Materials and methods

Materials

ALC-0315, ALC-0159, cholesteryl oleate, 1,2-di-*O*-octadecenyl-3-trimethylammonium propane (DOTMA), 1,2-dioleoyl-*sn-glycero*-3-phosphoethanolamine (DOPE), 1,2-distearoyl-*sn-glycero*-3-phosphorylcholine (DSPC), 1,2-distearoyl-*sn-glycero*-3-phosphoethanolamine–polyethylene glycol 2000 (DSPE–PEG) and triolein were purchased from MedChemExpress (Manmouth Junction, NJ, USA). Cholesterol, GelRed nucleic acid staining dye and Triton X-100 were sourced from Sigma-Aldrich (St. Loius, MN, USA). 6-(*p*-Toluidino)-2-naphthalenesulfonic acid sodium salt (TNS) was bought from Santa Cruz Biotechnology (Dallas, TA, USA). Plasmid DNA encoding firefly luciferase (FLuc pDNA, PGL4.51[luc2/CMV/Neo] vector), ONE-Glo Luciferase Assay reagent, VivoGlo luciferin, QuantiFluor RNA system and nuclease-free water were obtained from Promega Corporation (Madison, WI, USA). 5-Methoxyuridine-modified firefly luciferase mRNA (FLuc mRNA) was produced through a proprietary custom process at TriLink Bio Technologies (San Diego, CA, USA), while Cy5-tagged FLuc mRNA (Cy5-mRNA) was purchased from ApexBio Technology (Houston, TX, USA). AlamarBlue cell viability assay reagent, Hoechst 33342, LysoTracker Green DND-26 and Pierce detergent-compatible Bradford assay kit were procured from Thermo Fisher Scientific (Waltham, MA, USA). Lipofectamine 3000 (LF3000, Invitrogen, USA) was used per the manufacturer's protocol. All other chemicals and reagents were of analytical grade.

Preparation of iSLNs and cSLNs

The iSLN and cSLN formulations were prepared using an emulsification/solvent evaporation method. In brief, core structure lipids (cholesteryl oleate and triolein) and surface structure lipids (ALC-0315, DOTMA, DOPE and cholesterol) were co-dissolved in a chloroform/ethanol mixture (4 : 1, v/v) at specified weight ratios (Fig. 1B) with a total lipid concentration of 10 mg mL^{-1}. This solution (1 mL) was placed in a 15-mL conical tube. After adding 5 mL of nuclease free water, the mixture was vortexed for 10 s and sonicated for 2 min using an HTU Soni-130 ultrasonic homogenizer (20 kHz, 130 Watt). The oil-in-water emulsion was transferred to a 100-mL round-bottom flask and the solvents were evaporated with a Hei-VAP rotary evaporator (Heidolph, Germany) at 60 °C for 10 min. The final iSLN or cSLN suspensions in nuclease-free water were stored at 4 °C until use.

Formation of iSLN/mRNA and cSLN/mRNA complexes

iSLN in 5 μL of nuclease-free water was mixed with 100 ng of mRNA in 5 μL of nuclease-free water at various nitrogen-to-phosphate (N/P) ratios. The iSLN suspension and mRNA solution were mixed at 1 : 1 volume ratio. The mixture was incubated at 25 °C for 10 min to allow the formation of iSLN/mRNA complexes. For comparison, cSLN/mRNA complexes were prepared in the same manner.

Formation of iSLN/pDNA and cSLN/pDNA complexes

iSLN in 5 μL of nuclease-free water was mixed with 100 ng of pDNA in 5 μL of nuclease-free water at various N/P ratios. The iSLN suspension and pDNA solution were mixed at 1 : 1 volume ratio. The mixture was incubated at 25 °C for 10 min to allow the formation of iSLN/pDNA complexes. For comparison, cSLN/pDNA complexes were prepared in the same manner.

Formation of PEG-iSLN/mRNA and PEG-cSLN/mRNA complexes

The protocol for preparation of PEG-iSLNs or PEG-cSLNs was similar to that of iSLNs except that DSPE–PEG was included in the lipid mixture. The formed PEG-iSLN or PEG-cSLN in 5 μL of nuclease-free water was mixed with 100 ng of mRNA in 5 μL of nuclease-free water at a defined N/P ratio and incubated at 25 °C for 10 min to form PEG-iSLN/mRNA or PEG-cSLN/mRNA complexes.

Preparation of ALC-LNP

The benchmark ALC-LNP formulation was prepared using the same lipid composition as the BNT162b2 vaccine, as reported previously.[14] Briefly, mRNA in 10 mM sodium acetate buffer (pH 4.8) formed the aqueous phase, while lipids (ALC-0315 : DSPC : cholesterol : ALC-0159 at a molar ratio of 46.3 : 9.4 : 42.7 : 1.6) in ethanol created the organic phase. These phases (N/P ratio = 6) were manually mixed at 3 : 1 volume ratio using a pipette and incubated at 25 °C for 30 min to form ALC-LNPs. The ALC-LNPs were then buffer-exchanged with normal saline for *in vivo* use. Encapsulated mRNA was quantified using the QuantiFluor RNA system, with RNA concentration determined using a standard curve. Samples and standards (100 μL) in TE buffer were mixed with 100 μL of QuantiFluor RNA dye in a black-walled 96-well plate. After 5 min in the dark,

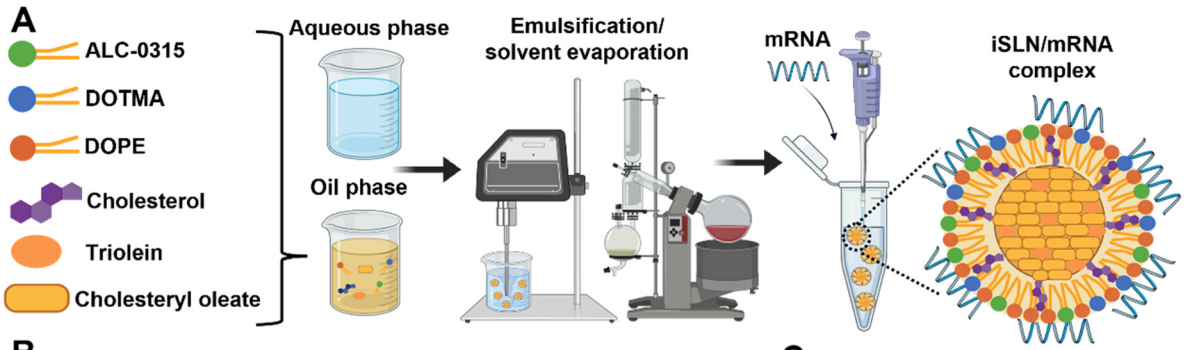

B

Formulations	Weight percentage (%)					
	Surface structure lipids				Core structure lipids	
	ALC-0315	DOTMA	DOPE	Cholesterol	Cholesteryl oleate	Triolein
iSLN-1	45	0	25	3	24	3
iSLN-2	34	11	25	3	24	3
iSLN-3	23	23	25	3	24	3
iSLN-4	11	34	25	3	24	3
cSLN	0	45	25	3	24	3

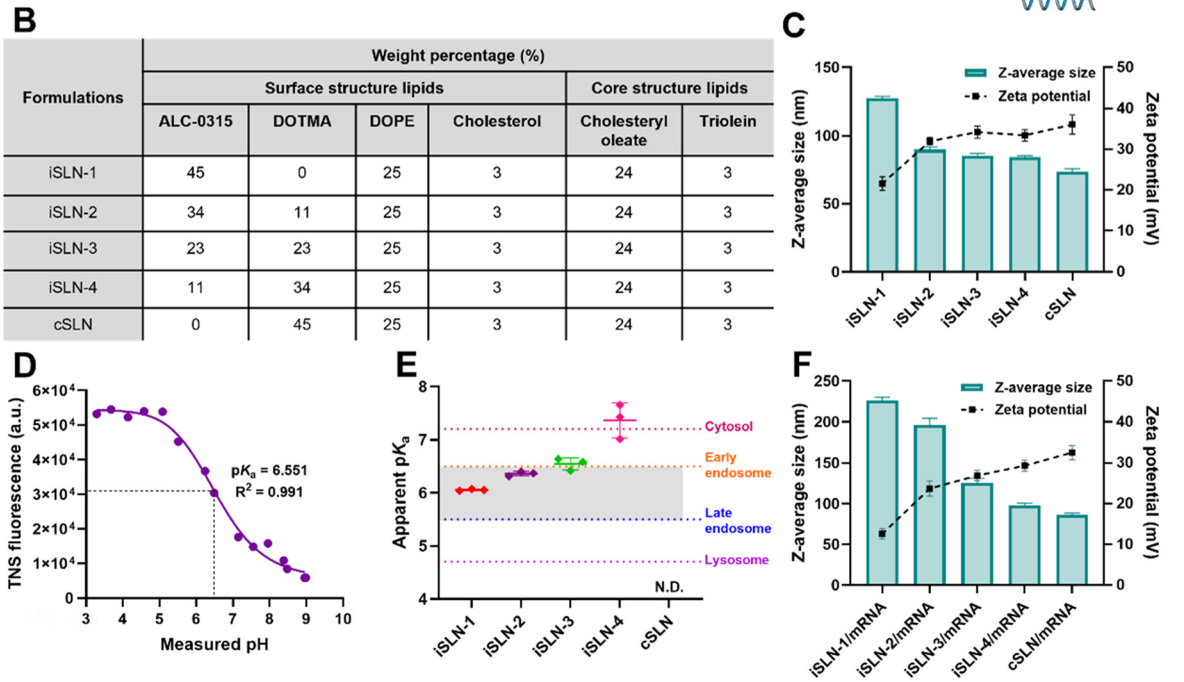

Fig. 1 Synthesis and characterization of bare iSLNs and iSLN/mRNA complexes. (A) Schematic for the self-assembly of bare iSLNs using an emulsification/solvent evaporation method and their complexation with mRNA *via* electrostatic interactions. (B) Tabulation of the composition of a series of iSLN and cSLN formulations. (C) *Z*-average size and zeta potential of bare iSLN and cSLN formulations. Mean ± SD (n = 3). (D) TNS fluorescence of iSLN-3 as a function of measured pH. pK_a was determined as the pH giving rise to half-maximal fluorescence intensity. (E) Comparison of the apparent pK_a values of iSLN and cSLN formulations. Early endosomal pH range (5.5–6.5) is marked by the gray area. N.D.: not detectable. Mean ± SD (n = 3). (F) *Z*-average size and zeta potential of iSLN/mRNA and cSLN/mRNA complexes formulated with FLuc mRNA at an N/P ratio of 6. Mean ± SD (n = 3).

fluorescence intensity was measured at 492 nm excitation and 540 nm emission using a Spark 10M microplate reader (Tecan, Switzerland). Encapsulation efficiency was calculated by comparing the QuantiFluor fluorescence before and after disrupting ALC-LNPs with 0.5% Triton X-100.

Nanoparticle characterization

The *Z*-average size, polydispersity index (PdI), and zeta potential of nanoparticle samples were analyzed using dynamic light scattering (DLS) on a Zetasizer Ultra Red (Malvern Panalytical, UK). iSLN/mRNA, cSLN/mRNA, PEG-iSLN/mRNA, and PEG-cSLN/mRNA complexes were formulated with FLuc mRNA, while iSLN/pDNA and cSLN/pDNA complexes were prepared with FLuc pDNA. All samples were diluted 10-fold for measurements. *Z*-average size and PdI were assessed in nuclease-free water, while zeta potential was measured in normal saline. All measurements were conducted in triplicate at 25 °C. For gel electrophoresis, all mRNA and pDNA complexes were formulated using FLuc mRNA and FLuc pDNA, respectively. These samples were run on a 1% agarose gel stained with GelRed in Tris-acetate–EDTA buffer at 100 V for 40 min, using RiboRuler high-range RNA ladder and 1 kb Plus DNA ladder (Thermo Fisher Scientific, USA) for size references. Gel images were captured with an iBright FL1500 Imaging System (Invitrogen, USA). The apparent pK_a values of iSLNs were determined by a TNS binding assay, as reported previously.[15]

Evaluation of mRNA translation efficiency and cell viability

The human embryonic kidney cell line HEK293T and mouse dendritic cell line DC2.4 (ATCC, USA) were maintained in 10% fetal bovine serum-supplemented DMEM and RPMI 1640 media, respectively. The cells were seeded in a white-walled 96-well plate at a density of 10^4 cells per well and incubated for 24 h. Afterward, the cells were treated with iSLN/mRNA, cSLN/

mRNA, PEG-iSLN/mRNA or PEG-cSLN/mRNA complexes formulated with 100 ng of FLuc mRNA at an N/P ratio of 6, which was the same as that used for ALC-LNP. For comparison, other wells were treated with ALC-LNP containing the same dose of FLuc mRNA (100 ng per well). Following 48 h of incubation, cells were rinsed with 100 μL of PBS and 50 μL of ONE-Glo Luciferase Assay reagent was added. After 3 min, the relative luminescence unit (RLU) of the cell lysate was measured on a Spark 10M microplate reader (Tecan group, Switzerland). The results were normalized to protein content, determined by the detergent-compatible Bradford assay kit and expressed as RLU per mg protein. To assess cell viability, a separate set of cells was seeded in a black-walled 96-well plate (10^4 cells per well) and treated with iSLN/mRNA, cSLN/mRNA, PEG-iSLN/mRNA, PEG-cSLN/mRNA complexes or ALC-LNP under the same conditions. After 48 h, cells were rinsed with PBS and incubated with 100 μL of AlamarBlue reagent (10% in culture media) for 2h. Fluorescence intensity (FI) was measured using the Spark 10M microplate reader with an excitation wavelength of 560 nm and an emission wavelength of 590 nm. Cell viability was expressed as a percentage of FI of analyzed cells relative to untreated controls.

Evaluation of pDNA translation efficiency and cell viability

pDNA translation efficiency and cell viability in HEK293T cells were evaluated following a protocol similar to that described for mRNA experiments. Briefly, cells were seeded in 96-well plates and treated after 24 h with iSLN/pDNA or cSLN/pDNA complexes, each containing 100 ng of FLuc pDNA at a specific N/P ratio. As a positive control, LF3000 was complexed with 100 ng of FLuc pDNA and used to treat the cells according to the manufacturer's protocol. After 48 h of incubation, luciferase activity was measured using the ONE-Glo Luciferase Assay, normalized to protein content and reported as RLU per mg protein. Cell viability was assessed in parallel using the AlamarBlue Assay and expressed relative to untreated controls.

Fusion activity test

The membrane fusion activity was assessed following previous literature with slight modifications.[16] Fresh blood was collected by submandibular bleeding from BALB/c mice and then washed with normal saline three times through repeated centrifugation at 1000 × *g* for 5 min at 4 °C. Next, 250 μL of erythrocyte suspension (2×10^8 cells per mL) was mixed with bare PEG-iSLN or PEG-cSLN formulations or their corresponding mRNA complexes diluted in PBS at pH 5.5, 6.5 or 7.4 to obtain a final lipid concentration of 30 μM. The same volume of normal saline and 1% Triton X-100 solution served as a negative and positive control, respectively. After incubating at 37 °C for 30 min, the suspension was centrifuged at 1000 × *g* for 5 min at 4 °C and the supernatant (100 μL) was carefully transferred to a transparent 96-well plate. The absorbance at 545 nm was measured using the Spark 10M microplate reader. The fusion activity was calculated using the following equation:

$$\text{Fusion activity (\%)} = \frac{[A_{\text{sample}} - A_{\text{NC}}]}{[A_{\text{PC}} - A_{\text{NC}}]} \times 100 \qquad (1)$$

where A_{PC}, A_{NC} and A_{sample} represent the absorbance values for the positive control, negative control and tested sample, respectively.

Confocal microscopy analysis of endosomal escape

DC2.4 cells were seeded at a density of 2×10^4 cells per well in a μ-slide 8 well chambered coverslip (Ibidi GmbH, Germany) and cultured for 24 h. Each well was then treated with ALC-LNP or PEG-iSLN-3/mRNA complexes containing 200 ng of Cy5-mRNA at an N/P ratio of 6. After 4 h incubation, cells were rinsed with 100 μL of PBS and stained with LysoTracker Green DND-26 (500 nM) for 1.5 h, followed by Hoechst 33342 (10 μg μL^{-1}) for 20 min.[17] After rinsing with PBS, cells were fixed with 4% paraformaldehyde for 15 min and observed using a LSM980 laser-scanning confocal microscope (Zeiss, Germany) equipped with a 63× oil-immersion objective lens. Mander's overlap coefficient (MOC) was used to quantify the co-localization between internalized Cy5-mRNA and endo-lysosomes. Co-localization analysis was performed on confocal images using JACoP (Just another co-localization plugin) in ImageJ 1.54g software (National Institutes of Health, USA).[18]

In vivo administration and bioluminescence imaging

All animal procedures were conducted according to the protocol 221681 approved by the Institutional Animal Care and Use Committee (IACUC) at the Biological Resource Centre of A*STAR, Singapore. Female BALB/c mice at the age of 5–6 weeks were purchased from InVivos Pte Ltd (Singapore) and then randomly divided into three groups that consisted of 3 mice each: ALC-LNP, PEG-iSLN-3/mRNA complexes and a mock control group. After intraperitoneal anesthesia with ketamine (75 mg kg^{-1})/xylazine (5 mg kg^{-1}), each mouse received either intramuscular or footpad subcutaneous injection of 40 μL of ALC-LNP or PEG-iSLN-3/mRNA complexes containing 1 μg of FLuc mRNA using BD Ultra-Fine II insulin syringes (30 gauge × 8 mm). Intramuscular injection was given to the thigh muscles of the left hind limb, whereas footpad subcutaneous injection was done at the palm of the left foot. At selected time points, each mouse was intraperitoneally injected with 200 μL of VivoGlo luciferin solution (15 mg mL^{-1} in PBS). In the case of footpad subcutaneous injection groups, additional 20 μL of VivoGlo luciferin solution was administered to the left footpad *via* a subcutaneous route. After 10-min stabilization, whole-body luminescence images were obtained on an IVIS Spectrum imaging system (Revvity, USA). The total flux values at each injection site were analyzed using Living Image Software (Revvity, USA).

Histology

Histological analysis was conducted at the Advanced Molecular Pathology Laboratory (AMPL), A*STAR. Female BALB/c mice were administered with PBS (mock control), ALC-LNP or

PEG-iSLN-3/mRNA complexes *via* intramuscular/footpad subcutaneous routes at the same dose used in the bioluminescence imaging study. At 4 h post administration, hind leg skeletal muscle and footpad tissues were harvested, fixed in 10% neutral buffered formalin, paraffin-embedded, and sectioned at 3 μm thickness for hematoxylin and eosin (H&E) staining. For immunohistochemical analysis, tissue sections were incubated with the rat anti-mouse Ly6G monoclonal antibody (HyCult Biotech #HM1039, 1 : 50) and goat anti-rat IgG-HRP conjugate (Abcam #ab97057, 1 : 100) was used as a secondary antibody for detection. The histological images were acquired using an IX83 inverted microscope (Olympus, Japan) and analyzed with ImageJ 1.54g software (National Institutes of Health, USA).

Statistical analyses

Graphs are represented as mean ± standard deviation (SD). GraphPad Prism 9.4.1 (GraphPad Software, USA) was used to perform statistical analyses *via* either one-way ANOVA followed by Tukey's *post hoc* test (for comparisons of three or more groups) or two-tailed unpaired Student's *t* test (for comparisons between two groups).

Results and discussion

Design, synthesis and characterization of iSLN/mRNA complexes

In this study, we attempted to design iSLN formulations by mimicking the chemical composition of high-density lipoproteins (HDLs). Natural HDLs have a core–shell structure composed of a nonpolar lipid core (cholesteryl esters and triglycerides) and a shell layer of polar phospholipids, cholesterol, and apolipoproteins.[19] In healthy individuals, HDLs typically consist of 24 wt% cholesteryl esters, 3 wt% triglycerides, 45 wt% apolipoproteins, 25 wt% phospholipids and 3 wt% cholesterol.[20] For iSLN formulations, 45 wt% apolipoproteins and 25 wt% phospholipids present in natural HDL were replaced with 45 wt% ALC-0315/DOTMA mixture and 25 wt% DOPE, respectively, while keeping the other constituents the same (Table 1). ALC-0315 is a clinically validated ionizable lipid widely used in mRNA and pDNA delivery systems for its ability to form stable complexes and enable efficient transfection both *in vitro* and *in vivo*.[21] DOTMA is a quaternary ammonium-based cationic lipid that has been used to formulate lipoplexes for systemic mRNA and pDNA delivery.[22,23] The fusogenic lipid DOPE was chosen to reconstitute the phospholipid portion because of its ability to destabilize the endosomal membrane *via* the formation of an inverted hexagonal phase in an acidic environment.[24] Cholesteryl oleate having a melting point of 47 °C was incorporated to form the solid lipid matrix of iSLNs at physiological temperature.[25] This cholesteryl derivative has previously been reported to attenuate cytotoxicity and improve transfection efficiency of cSLN-nucleic acid complexes.[26] Triolein was selected to reconstitute the triglyceride portion based on the finding that most of HDL triglycerides contain oleic moieties.[27] Fig. 1A illustrates the iSLN formulation process, where all lipid components co-dissolved in a chloroform/ethanol mixture were added into nuclease-free water and then subjected to ultrasonication to form an oil-in-water (O/W) emulsion. Upon solvent evaporation, hydrophobic interactions between lipid molecules would induce the self-assembly of iSLNs with a spherical core–shell structure, where a nonpolar lipid core composed of cholesteryl oleate and triolein is surrounded by an amphipathic shell layer of ALC-0315/DOTMA mixture, DOPE and cholesterol. Owing to the positively charged shell layer, negatively charged mRNA molecules would be adsorbed on the surface of iSLNs *via* electrostatic interactions, resulting in the formation of nanosized ionic complexes.

Table 1 Chemical composition of natural HDL and iSLN formulations

	Natural HDL		iSLN	
	Constituent	Weight (%)	Constituent	Weight (%)
Core	Cholesteryl esters	24	Cholesteryl oleate	24
	Triglyceride	3	Triolein	3
Surface	Apolipoproteins	45	ALC-0315 + DOTMA	45
	Phospholipids	25	DOPE	25
	Cholesterol	3	Cholesterol	3

We synthesized a series of iSLNs with varying weight ratios of ALC-0315 to DOTMA (Fig. 1B). A pure ALC-0315-based formulation named iSLN-1 was prepared using 45 wt% ALC-0315 (*i.e.* 45% of the total lipid weight). Three additional formulations named iSLN-2 to iSLN-4 were synthesized by varying the ALC-0315 : DOTMA ratio from 3 : 1 to 1 : 3, while keeping the weight ratio of the other four components constant (DOPE/cholesterol/cholesteryl oleate/triolein = 25/3/24/3). For comparison, a pure DOTMA-based formulation named cSLN was prepared by replacing ALC-0315 in iSLN-1 with an equal weight percentage (45 wt%) of DOTMA. Increasing the weight percentage of DOTMA resulted in a gradual increase in the zeta potential of iSLNs from ~22 mV to ~36 mV, with an accompanying decrease in their *Z*-average size from ~128 nm to ~74 nm (Fig. 1C). Next, apparent pK_a values of iSLN formulations were measured by the TNS binding assay. As shown in Fig. 1D, TNS fluorescence of iSLN-3 increased sharply as the pH dropped below the pK_a, indicating the protonation of ionizable amine groups.[15] On the other hand, no obvious pH transition was detected from cSLN lacking an ionizable tertiary amine moiety (Fig. S1). Of note, the pK_a of iSLNs could be adjusted from approximately 6.05 to 7.43 by increasing the DOTMA content from 0 to 34 wt% (Fig. 1E). Given their pK_a values lying within the early endosomal pH range (5.5–6.5), iSLN-1 to -3 were anticipated to be able to escape early endosomes to facilitate transport of nucleic acid payloads to the cytoplasm.[4] DLS analysis of iSLN/mRNA complexes revealed that electrostatic adsorption of mRNA increased the particle size with a concomitant decrease in the surface charge (Fig. 1F). The electrophoretic mobility of mRNA was fully retarded upon mixing with iSLNs and cSLN, indicative of their complete complexation with mRNA (Fig. S2). Storage stability is a crucial factor for practical applications of nucleic acid delivery systems. Encouragingly, all iSLNs and cSLN showed negligible variations

in the *Z*-average size, PdI and zeta potential during storage at 4 °C for 18 months (Fig. S3). The observed long-term storage stability might be attributed to the highly crystalline state of solid lipid matrices in SLN dispersions.[28]

Evaluation of the applicability of iSLNs for mRNA and pDNA transfection

The translation efficiency and cytotoxicity of iSLN/mRNA complexes formulated with firefly luciferase reporter mRNA (FLuc mRNA) were evaluated on HEK293T and DC2.4 cell lines. Given the fast-growing nature and relatively high protein productivity, the HEK293T cell line has been widely used for large-scale production of human recombinant proteins and biopharmaceuticals.[29] DC2.4 is a cell line exhibiting characteristic features of dendritic cells, such as cross-presentation ability.[30] Notably, the weight ratio of ALC-0315 to DOTMA was found to have a significant impact on the transfection efficiency of iSLN/mRNA complexes in both HEK293T and DC2.4 cell lines (Fig. 2A and B). For example, FLuc expression levels gradually increased as the ALC-0315 : DOTMA ratio was decreased from 4 : 0 to 2 : 2, but a further decrease of this ratio led to a decline in FLuc expression levels. Encouragingly, although iSLN/mRNA mediated lower FLuc expression levels in HEK293T cells compared to the benchmark ALC-LNP, iSLN-3/mRNA complexes exhibited significantly higher transfection efficiency ($P < 0.0001$) in DC2.4 cells. This suggests the existence of an optimal ratio of ALC-0315 to DOTMA that maximizes the mRNA translation efficiency of iSLNs. No obvious cytotoxicity was detected from all iSLN formulations, indicating that the combination of ALC-0315 and DOTMA did not negatively affect the viability of the transfected HEK293T and DC2.4 cells (Fig. 2C and D).

Next, we explored the potential of iSLN formulations for intracellular delivery of plasmid DNA (pDNA) in HEK293T cells. The pDNA encoding firefly luciferase reporter (FLuc pDNA) was mixed with iSLNs to form iSLN/pDNA complexes *via* electrostatic interactions. Elevating the DOTMA fraction caused a gradual increase in the zeta potential of iSLN/pDNA and cSLN/pDNA complexes from ~22 mV to ~37 mV, with a concomitant reduction in their *Z*-average size from ~118 nm to ~76 nm (Fig. S4A). The transfection efficiencies of iSLN-3/pDNA complexes were first tested at various N/P ratios ranging from 2 to 14 in HEK293T cells. As shown in Fig. 3A, luciferase expression levels increased steadily from N/P ratio 2 to 12 and then dropped at a N/P ratio of 14. No cytotoxicity was observed across all tested N/P ratios (Fig. 3B). Based on these findings, an N/P ratio of 12 was chosen to evaluate the applicability of iSLN formulations for pDNA delivery. Gel electrophoresis confirmed that pDNA was fully complexed with all iSLNs and cSLN at the selected N/P ratio of 12 (Fig. S4B). As presented in Fig. 3C, the ALC-0315:DOTMA ratio had a substantial influence on pDNA transfection efficiency of iSLNs. Consistent with our findings

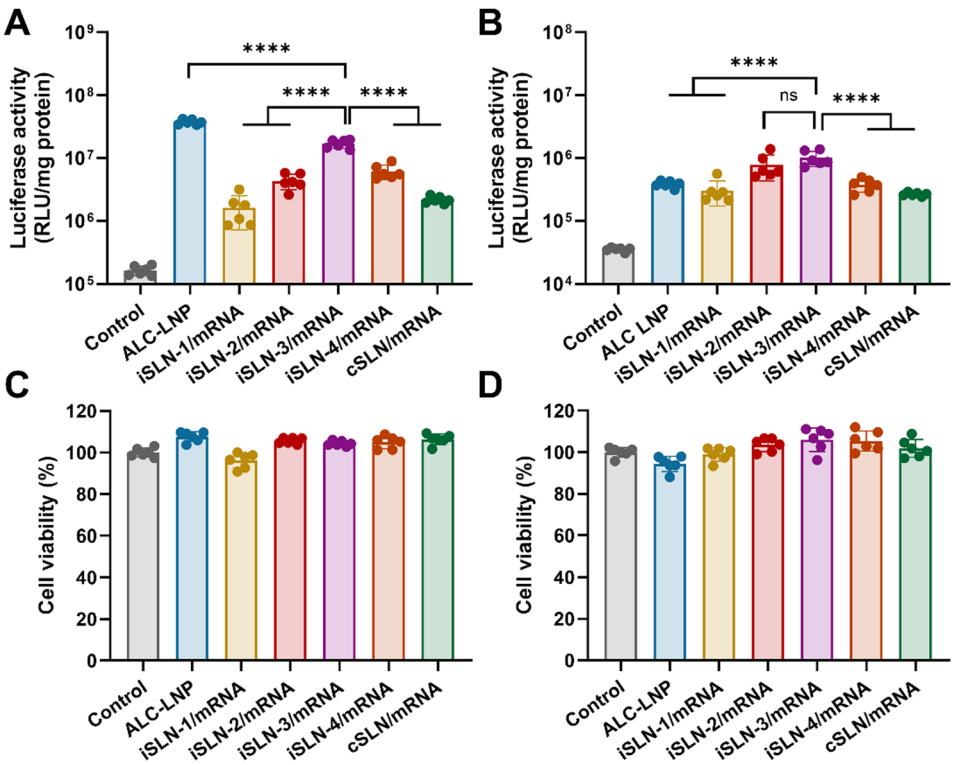

Fig. 2 *In vitro* translation efficiency of iSLN/mRNA and cSLN/mRNA complexes. Luciferase expression levels of (A) HEK293T and (B) DC2.4 cells treated for 48 h with ALC-LNP, iSLN/mRNA or cSLN/mRNA complexes formulated with FLuc mRNA at an N/P ratio of 6. Mean ± SD (n = 6); ****P <0.0001; ns: nonsignificant. Viability of (C) HEK293T and (D) DC2.4 cells treated for 48 h with ALC-LNP, iSLN/mRNA or cSLN/mRNA complexes formulated with FLuc mRNA (N/P ratio = 6). Mean ± SD (n = 6).

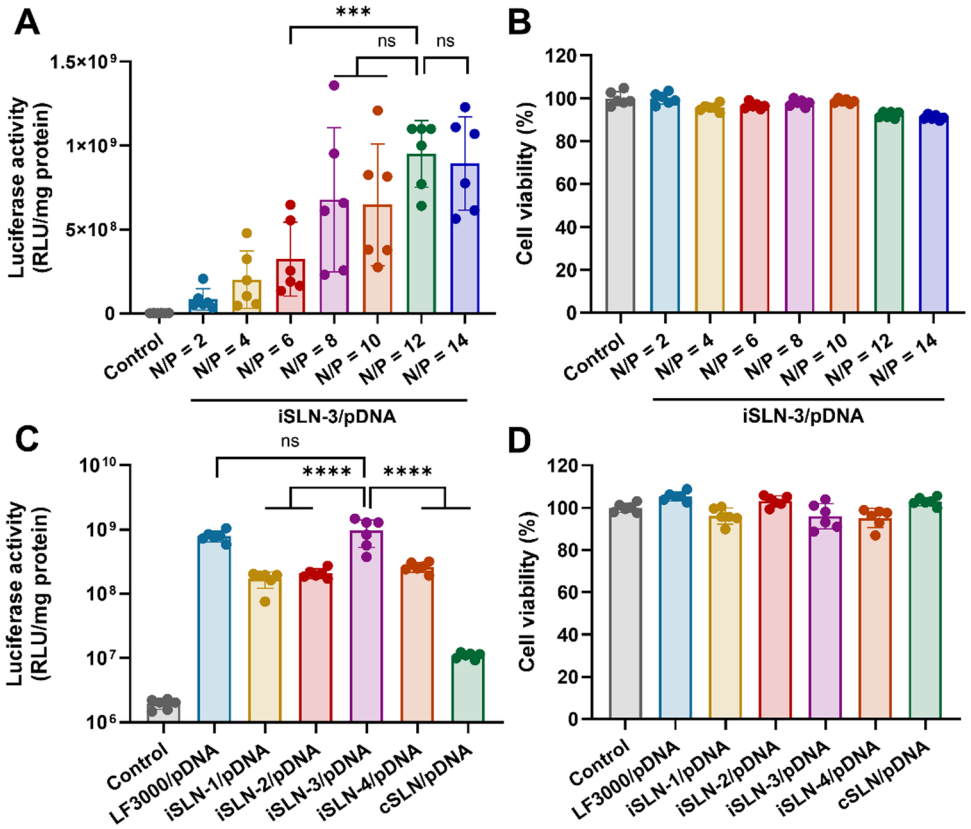

Fig. 3 *In vitro* translation efficiency of iSLN/pDNA and cSLN/pDNA complexes. (A) Luciferase expression levels and (B) viability of HEK293T cells treated for 48 h with iSLN-3/pDNA complexes formulated with FLuc pDNA at various N/P ratios from 2 to 14. Mean ± SD (n = 6); ***P < 0.001; ns: nonsignificant. (C) Luciferase expression levels and (D) viability of HEK293T cells treated for 48 h with LF3000/pDNA, iSLN/pDNA or cSLN/pDNA complexes formulated with FLuc pDNA at an N/P ratio of 12. Mean ± SD (n = 6); ****P < 0.0001; ns: nonsignificant.

from iSLN/mRNA complexes, FLuc pDNA expression levels peaked for iSLN-3, which was formulated at an ALC-0315 : DOTMA ratio of 2 : 2. Impressively, iSLN-3 achieved pDNA transfection efficiency comparable to that of the commercially available LF3000 reagent. All tested iSLN formulations did not cause any noticeable cytotoxicity against HEK293T cells (Fig. 3D). The above results demonstrated the potential of iSLNs as efficient and nontoxic transfection agents for various nucleic acid drugs including pDNA and mRNA.

Characterization and *in vitro* translation efficiency of PEGylated iSLN/mRNA complexes

PEGylation, the process of coating with polyethylene glycol (PEG), has been widely employed to enhance nanoparticle stability and bioavailability by minimizing aggregation, non-specific protein adsorption and phagocytic clearance.[31] In our study, iSLN-3 was selected for PEGylation because it exhibited the highest transfection efficiency among all iSLN formulations. To determine the optimal PEG coating density, iSLN-3 was formulated with various DSPE–PEG contents (0.5, 1 and 1.5 mol%). The introduction of 0.5 mol% DSPE–PEG did not compromise the pDNA translation efficiency of iSLN-3, but a further increase in DSPE–PEG contents to 1.5 mol% markedly diminished FLuc expression levels without noticeable cytotoxicity (Fig. S5). This result is in good agreement with the literature reporting the detrimental effect of PEG on the cellular uptake of lipid nanoparticles.[32,33]

On the basis of this finding, PEGylated iSLNs (PEG-iSLNs) containing DSPE–PEG at 2 wt%, which corresponds to 0.5 mol% of the total lipids (Table 2), were chosen for subsequent experiments. Since the initial DSPE–PEG mol% optimization was based on pDNA complexes, the entire PEG-iSLN series was formulated to screen for mRNA delivery, as mRNA and pDNA have distinct intracellular pathways that can influence translation efficiency.[21] As shown in Fig. 4A, PEG-iSLNs had slightly larger sizes and more neutralized zeta potential in comparison to their non-PEGylated counterparts, reflecting the presence of neutral-charged PEG chains on the particle surface.[34] Similar to our observation on iSLN/mRNA complexes, higher zeta potential and smaller Z-average size of PEG-iSLN/mRNA complexes were detected at greater weight percentages of DOTMA. No free mRNA was detected in all PEG-iSLN/mRNA complexes in the gel electrophoresis assay, verifying the complete mRNA condensation (Fig. S6). Only a marginal variation in the Z-average size, PdI and zeta potential was observed across all PEG-iSLN formulations even after 12 months of storage at 4 °C, indicative of their stability under long-term storage conditions (Fig. S7). The transfection efficiencies of PEG-iSLN/mRNA and PEG-cSLN/mRNA complexes were evaluated in HEK293T and DC2.4 cells (Fig. 4B and C). Consistent with our earlier findings,

Table 2 Lipid composition of a series of PEG-iSLN and PEG-cSLN formulations

	Weight percentage (%)						
	Surface structure lipids					Core structure lipids	
Formulations	ALC-0315	DOTMA	DOPE	Cholesterol	DSPE–PEG	Cholesteryl oleate	Triolein
PEG-iSLN-1	44	0	24	3	2	24	3
PEG-iSLN-2	33	11	24	3	2	24	3
PEG-iSLN-3	22	22	24	3	2	24	3
PEG-iSLN-4	11	33	24	3	2	24	3
PEG-cSLN	0	44	24	3	2	24	3

PEG-iSLN-3, formulated with an ALC-0315 : DOTMA ratio of 2 : 2, significantly ($P < 0.0001$) outperformed PEG-iSLN-1 (ALC-0315 alone) and PEG-cSLN (DOTMA alone) in both cell lines. Notably, PEG-iSLN-3 was much more effective than ALC-LNP at delivering mRNA to DC2.4 cells. No severe cytotoxicity was observed with all PEG-iSLN/mRNA formulations (Fig. 4D and E).

Assessment of the fusion activity of PEG-iSLN/mRNA complexes

To elucidate the mechanism of the transfection mediated by PEG-iSLN/mRNA complexes, their membrane fusion activity was assessed at three different pH values: 7.4 (extracellular space), 6.5 (early endosome) and 5.5 (late endosome).[16] We first assessed the membrane fusion activity of bare PEG-iSLNs and observed that the ALC-0315 : DOTMA ratio strongly influenced their pH-responsive membrane-disruptive behaviour (Fig. S8). For example, the hemolytic activity of PEG-iSLN-3, PEG-iSLN-4 and PEG-cSLN was higher than that of PEG-iSLN-1 and PEG-iSLN-2 at pH 7.4 due to a greater amount of cationic lipid DOTMA present in these formulations. The membrane fusion activity of PEG-iSLN-1 to -3 was greatly enhanced when the pH dropped from 7.4 to 5.5, whereas PEG-iSLN-4 and PEG-cSLN showed only slight changes in the hemolytic activity. This difference is likely attributed to the higher ALC-0315 content in PEG-iSLN-1 to -3, which helps disrupt erythrocyte membranes *via* the acquisition of positive charges at acidic pH.[35] PEG-iSLN/mRNA complexes followed a similar pH-responsive trend as their bare counterparts, suggesting that mRNA complexation did not substantially affect the membrane-disrupting properties of PEG-iSLNs (Fig. 5A). Notably, the hemolytic activity of PEG-iSLN-3/mRNA complexes was markedly ($P < 0.0001$) augmented from pH 7.4 to 6.5, highlighting their superior ability to disrupt the bilayer membrane in response to the early endosomal environment.[18,36] Considering that the pK_a of SLN-3

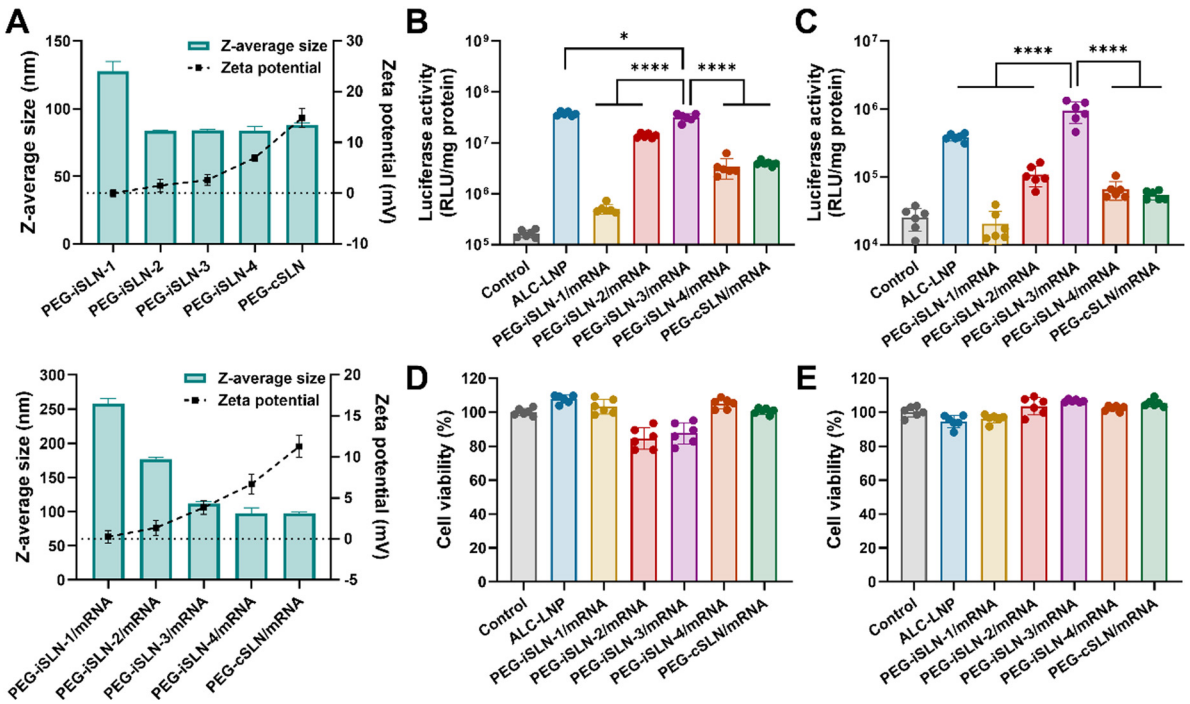

Fig. 4 Characterization and *in vitro* translation efficiency of PEG-iSLN/mRNA and PEG-cSLN/mRNA complexes. (A) *Z*-average size and zeta potential of bare PEG-iSLNs and their complexes with FLuc mRNA. Mean ± SD ($n = 3$). Luciferase expression levels of (B) HEK293T and (C) DC2.4 cells treated for 48 h with ALC-LNP, PEG-iSLN/mRNA or PEG-cSLN/mRNA complexes formulated with FLuc mRNA at an N/P ratio of 6. Mean ± SD ($n = 6$). *$P < 0.05$; ****$P < 0.0001$. Viability of (D) HEK293T and (E) DC2.4 cells treated for 48 h with ALC-LNP, PEG-iSLN/mRNA or PEG-cSLN/mRNA complexes formulated with FLuc mRNA (N/P ratio = 6). Mean ± SD ($n = 6$).

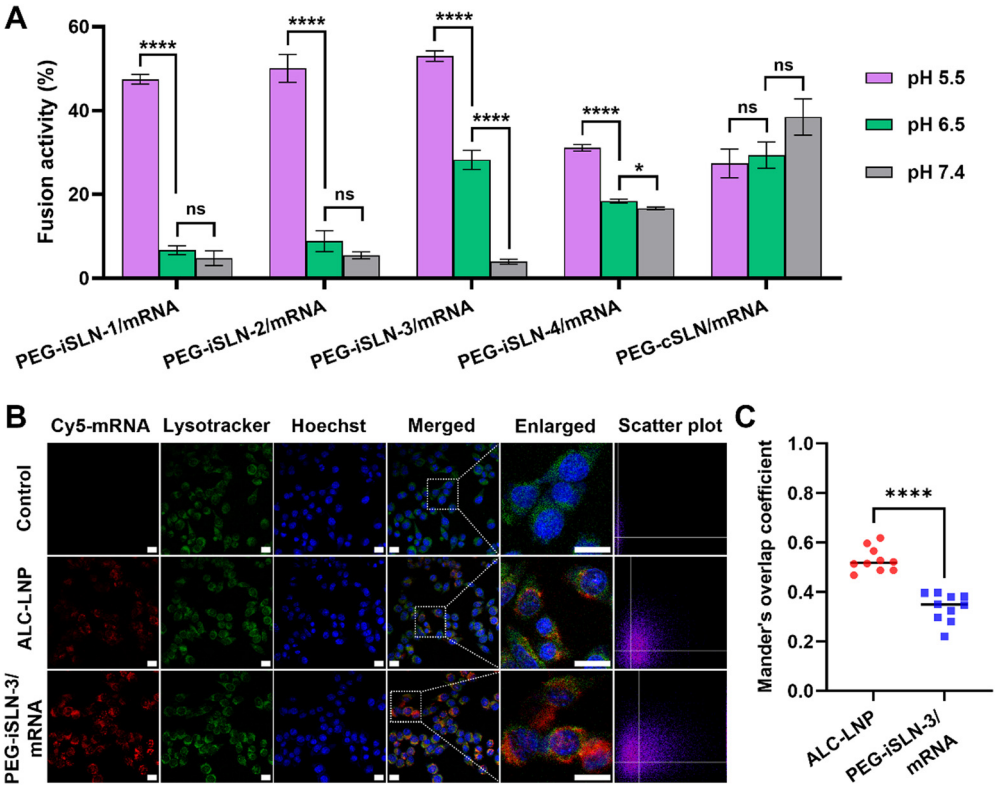

Fig. 5 Acidic pH-sensitive, membrane-disruptive behaviour of PEG-iSLN/mRNA complexes. Evaluation of the membrane fusion activity of (A) PEG-iSLN/mRNA or PEG-cSLN/mRNA complexes measured at various pH (5.5, 6.5 or 7.4). Mean ± SD (n = 3); ****$P < 0.0001$; *$P < 0.05$; ns: nonsignificant. (B) Confocal microscopy images of DC2.4 cells at 4 h post-transfection of ALC-LNP or PEG-iSLN-3/mRNA complexes formulated with Cy5-mRNA (red). The endosomes and cell nuclei were stained with Lysotracker Green DND-26 (green) and Hoechst 33342 dye (blue), respectively. Scale bars: 20 μm. The scatter plots show the relationship between the fluorescence signals in red and green channels. (C) Mander's overlap coefficient (MOC) between the endosomes and either ALC-LNP or PEG-iSLN-3/mRNA complexes. MOC values were acquired from 10 different cells per group using ImageJ software. Mean ± SD (n = 10); ****$P < 0.0001$.

(6.55) is higher than those of iSLN-1 (6.06) and -2 (6.36), PEG-iSLN-3/mRNA complexes are expected to acquire a positive surface charge as soon as they reach the early endosome with pH < 6.5, facilitating timely endosomal escape and cytosolic mRNA delivery.[12] On the other hand, PEG-iSLN-4 and PEG-cSLN/mRNA complexes formulated with less ALC-0315 content showed no substantial increase in fusion activity at pH 6.5, suggesting that an optimally balanced ionizable/cationic lipid content plays an important role in mediating the effective destabilization of the bilayer membrane in response to the early endosomal pH.[37]

Next, we conducted a confocal microscopy study to investigate the endosomal escape of PEG-iSLN-3/mRNA complexes in DC2.4 cells. Cy5-mRNA was employed to track the subcellular localization of ALC-LNP and PEG-iSLN-3/mRNA complexes, while Lysotracker Green DND-26 and Hoechst 33342 dyes were used to visualize the endosomes and cell nuclei, respectively. Some fractions of Cy5-mRNA-loaded ALC-LNP (red) were sequestered in endosomal compartments (green), as identified by yellow regions in the merged channel images (Fig. 5B). Notably, considerably lower colocalization was observed between endosomes and PEG-iSLN-3/mRNA complexes, indicative of their superior endosome-escaping ability.

This observation was further supported by a significant ($P < 0.0001$) decrease in the Mander's overlap coefficient (MOC) for PEG-iSLN-3/mRNA complexes (0.34 ± 0.06) compared to ALC-LNP (0.53 ± 0.05; Fig. 5C). The above results revealed that PEG-iSLN-3/mRNA complexes effectively facilitated the endosomal destabilization and subsequent delivery of mRNA payloads into the cytoplasm *via* their acidic pH-sensitive membrane-fusion activity.

In vivo mRNA delivery performance and local tissue reaction of PEG-iSLN-3/mRNA complexes

Bioluminescence imaging study was performed to examine the *in vivo* mRNA delivery performance of the leading candidate PEG-iSLN-3/mRNA complexes. We tested two routes of administration (intramuscular and footpad subcutaneous injection; Fig. 6A), which are commonly used for vaccination studies in mouse models.[38,39] When FLuc mRNA-loaded ALC-LNP was administered to BALB/c mice *via* an intramuscular route, intense luminescence signal was detected at both the hind leg muscle (injection site) and liver at 4 h post-injection (Fig. 6B), which is consistent with previous literature.[40] On the other hand, the luminescence signal of PEG-iSLN-3/mRNA complexes given at the same dose (1 μg mRNA/mouse) was

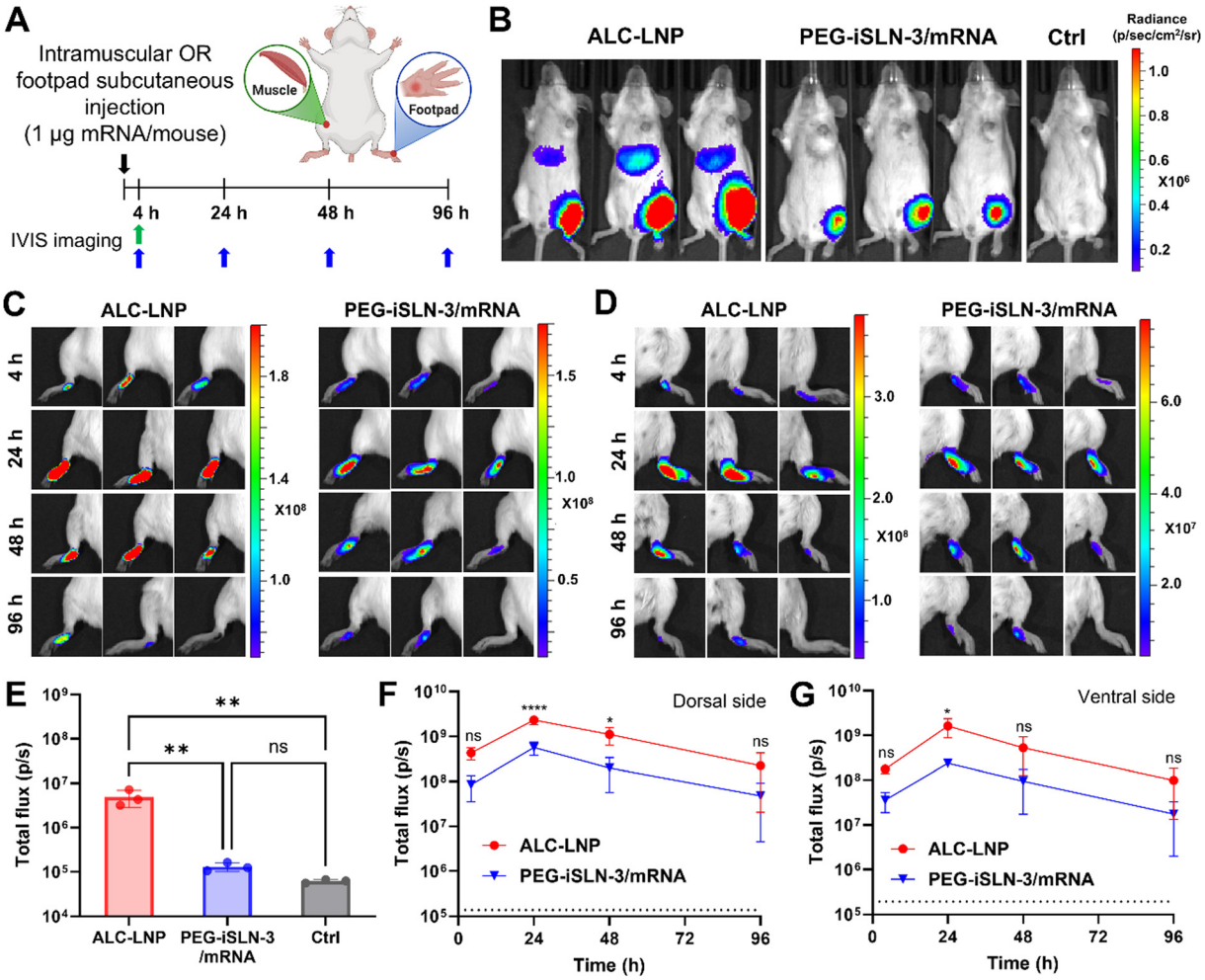

Fig. 6 *In vivo* mRNA translation profiles of ALC-LNP and PEG-iSLN-3/mRNA complexes in BALB/c mice. (A) Experiment timeline for intramuscular/footpad subcutaneous administration and subsequent IVIS imaging. Created with BioRender.com. (B) Whole-body bioluminescence images of BALB/c mice taken at 4 h after intramuscular injection of ALC-LNP or PEG-iSLN-3/mRNA complexes at the same dose (1 μg of FLuc mRNA/mouse). Naive mice that received only luciferin solution were used as a mock control (Ctrl). (C) Dorsal and (D) ventral bioluminescence images of the left foot of BALB/c mice taken at 4, 24, 48 and 96 h after footpad subcutaneous injection of ALC-LNP or PEG-iSLN-3/mRNA complexes (1 μg of FLuc mRNA/mouse). (E) Total flux values of the liver of BALB/c mice following the intramuscular administration. Mean ± SD (n = 3); $^{**}P < 0.01$; ns: nonsignificant. Time-course changes in total flux values in the left foot of BALB/c mice on the (F) dorsal and (G) ventral sides following the footpad subcutaneous administration. The dotted line represents the limit of detection. Mean ± SD (n = 3); $^{****}P < 0.0001$; $^{*}P < 0.05$; ns: nonsignificant.

highly concentrated at the leg muscle, while showing minimal signal in the liver region. The total flux quantification also showed that PEG-iSLN-3/mRNA complexes exhibited a significantly lower FLuc signal in the liver compared to ALC-LNP ($P < 0.01$; Fig. 6E). It has been reported that liver injury frequently occurs following vaccination with COVID-19 mRNA vaccines (*e.g.*, BNT162b2 and mRNA-1273).[41,42]

A recent study has suggested that liver injury might be associated with the increased uptake of ALC-0315 into hepatocytes and hepatic stellate cells.[43] From this perspective, the minimal liver accumulation of PEG-iSLN-3/mRNA complexes would help avoid the unwanted hepatotoxicity.

Intriguingly, upon footpad subcutaneous injection, the FLuc signal of ALC-LNP and PEG-iSLN-3/mRNA complexes was visible only at the injection site (Fig. S9). As depicted in Fig. 6C and D, the luminescence signal for both groups peaked at 24 h and then declined by 96 h on the dorsal and ventral sides. This observation was further supported by the total flux measurements, which showed that FLuc mRNA translation peaked at 24 h and gradually returned to initial values over 96 h on the dorsal (Fig. 6F) and ventral (Fig. 6G) regions. Notably, ALC-LNP showed higher luminescence signal compared to PEG-iSLN-3/mRNA complexes across all time points. A similar trend was also observed for the leg muscle following intramuscular administration (Fig. S10). This observation does not align with our *in vitro* studies, where PEG-iSLN-3/mRNA complexes exhibited greater transfection efficiency and endosomal escape than ALC-LNP in DC2.4 cells. The observed discrepancy between *in vitro* and *in vivo* outcomes is foreseeable as *in vitro* cell culture conditions cannot fully replicate the complex physiological barriers present *in vivo*.[44–46]

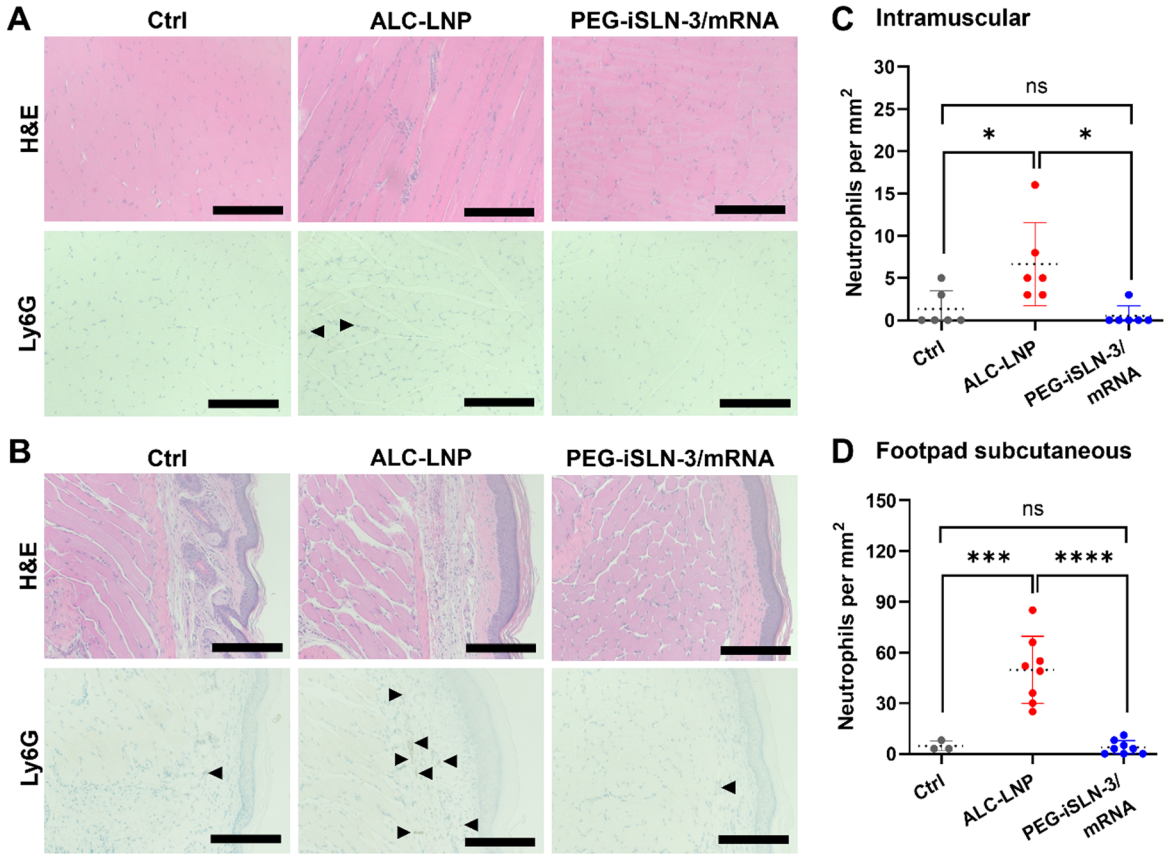

Fig. 7 Local tissue reaction following intramuscular/footpad subcutaneous administration of ALC-LNP and PEG-iSLN-3/mRNA complexes. Representative H&E and Ly6G (neutrophil marker) staining of (A) hind leg skeletal muscle and (B) footpad tissues collected 4 h after intramuscular or footpad subcutaneous administration of ALC-LNP and PEG-iSLN-3/mRNA complexes. Ly6G-positive cells are marked by black arrow heads. Scale bar: 200 μm. Quantification of neutrophils in (C) skeletal muscle and (D) footpad was performed using ImageJ software. Mean ± SD (n = 3-6 for Ctrl, n = 6-8 for ALC-LNP and PEG-iSLN-3/mRNA); *P < 0.05; ***P < 0.001; ****P < 0.0001; ns: nonsignificant (one-way ANOVA with Tukey's *post hoc* test).

To assess local tissue reaction following administration, we conducted H&E and immunohistochemical staining (for Ly6G; neutrophil marker) of tissue specimens collected from the injection sites. We observed a marked recruitment of neutrophils in both intramuscular and footpad subcutaneous spaces of the mice at 4 h-post injection of ALC-LNP (Fig. 7A and B). In contrast, no apparent neutrophil accumulation was observed in the mice treated with PEG-iSLN-3/mRNA complexes, suggesting that they caused only a minimal level of local inflammation. Our findings were further supported by quantified neutrophil counts, where the number of neutrophils was significantly increased only in the ALC-LNP group (Fig. 7C and D). This is in agreement with a previous study, in which intramuscular injection of mRNA-LNP induced a strong local inflammation characterized by neutrophil recruitment.[47] Notably, the inflammatory response of mRNA-LNP has been shown to be dependent on its ionizable lipid component.[47,48] In our study, although PEG-iSLN-3 formulation also contains the ionizable lipid ALC-0315, the administered dose per mouse was considerably lower (PEG-iSLN-3/mRNA complexes: 6.3 μg *vs.* ALC-LNP: 13.6 μg), which may explain the observed differences in the local tissue reaction. In addition, the reduced inflammation observed with PEG-iSLN-3/mRNA complexes might be related to the presence of triolein, which has been previously reported to possess anti-inflammatory properties.[49] Overall, these findings demonstrated the potential applicability and safety of PEG-iSLN-3/mRNA complexes for *in vivo* mRNA delivery *via* both intramuscular and footpad subcutaneous routes.

Conclusions

By mimicking the chemical composition of HDLs, we designed a series of iSLNs with varying weight ratios of ALC-0315 and DOTMA. Control of the ionizable/cationic lipid ratios enabled the fine-tuning of the apparent pK_a of iSLNs to the early endosomal pH range. Notably, iSLN-3 and its PEGylated counterpart (PEG-iSLN-3), formulated at an ALC-0315/DOTMA ratio of 2 : 2, exhibited superior mRNA transfection efficiency compared to formulations with either ALC-0315 or DOTMA alone *in vitro*. Mechanistic studies revealed that PEG-iSLN-3/mRNA complexes promoted endosomal destabilization and efficient cytoplasmic delivery of mRNA due to their ability to disrupt the bilayer membrane in response to the mildly acidic early endosomal environment. Moreover, bioluminescence imaging demonstrated effective *in vivo* mRNA delivery *via* PEG-iSLN-3/mRNA complexes through two common routes of vaccination:

intramuscular and footpad subcutaneous administration. Histological analysis confirmed that PEG-iSLN-3/mRNA complexes induced minimal local inflammation. Additionally, both iSLNs and PEG-iSLNs exhibited remarkable stability during storage over 12 months at 4 °C. Overall, these findings establish PEG-iSLN formulations as promising carriers for the delivery of diverse nucleic acid cargoes in future therapeutic applications.

Author contributions

Y. Y. Y. and K. H. B. were involved in conception and design of the study. N. M. conducted nanoparticle synthesis and *in vitro* characterization experiments. N. M., K. H. B. and J. L. performed animal experiments. N. M. and K. H. B. performed data analysis and drafted the manuscript. J. H. P. H. and Y. Y. Y. provided guidance and edited the manuscript. Y. Y. Y. supervised the project. All authors reviewed and approved the final manuscript.

Conflicts of interest

There are no conflicts to declare.

Data availability

The data that support the findings of this study are available from the corresponding author upon reasonable request.

Supplementary information available: Representative TNS fluorescence titration curves, gel electrophoresis analysis of SLN/mRNA or pDNA nanocomplexes with or without PEG, size, PDI and zeta potential, luciferase expression levels and viability of HEK293T cells treated with PEG-iSLN-3/pDNA nanocomplexes, fusion activity of PEG-iSLN or PEG-cSLN formulations, whole body images of mice at 4 h after s.c. injection of ALC-LNP or PEG-iSLN-3/mRNA nanocomplexes, total flux values of the hind leg muscle (injection site) of mice following intramuscular administration of ALC-LNP or PEG-iSLN-3/mRNA nanocomplexes. See DOI: **https://doi.org/10.1039/d5tb00470e**

Acknowledgements

This work was supported by the Bioprocessing Technology Institute (BTI), A*STAR, IAF-PP grant (H22J1a0050) and NRF-CRP grant (CRP27-2021-0038), Republic of Singapore. N. M. acknowledges the support from A*STAR for the SINGA scholarship. The graphical abstract was created with BioRender.com.

References

1 A. Akinc, M. A. Maier, M. Manoharan, K. Fitzgerald, M. Jayaraman, S. Barros, S. Ansell, X. Du, M. J. Hope, T. D. Madden, B. L. Mui, S. C. Semple, Y. K. Tam, M. Ciufolini, D. Witzigmann, J. A. Kulkarni, R. van der Meel and P. R. Cullis, *Nat. Nanotechnol.*, 2019, **14**, 1084–1087.
2 L. Schoenmaker, D. Witzigmann, J. A. Kulkarni, R. Verbeke, G. Kersten, W. Jiskoot and D. J. A. Crommelin, *Int. J. Pharm.*, 2021, **601**, 120586.
3 X. Han, H. Zhang, K. Butowska, K. L. Swingle, M. G. Alameh, D. Weissman and M. J. Mitchell, *Nat. Commun.*, 2021, **12**, 7233.
4 E. Blanco, H. Shen and M. Ferrari, *Nat. Biotechnol.*, 2015, **33**, 941–951.
5 R. Tenchov, R. Bird, A. E. Curtze and Q. Zhou, *ACS Nano*, 2021, **15**, 16982–17015.
6 M. B. de Jesus and I. S. Zuhorn, *J. Controlled Release*, 2015, **201**, 1–13.
7 C. Botto, G. Augello, E. Amore, M. R. Emma, A. Azzolina, G. Cavallaro, M. Cervello and M. L. Bondi, *J. Biomed. Nanotechnol.*, 2018, **14**, 1009–1016.
8 S. Doktorovova, D. L. Santos, I. Costa, T. Andreani, E. B. Souto and A. M. Silva, *Int. J. Pharm.*, 2014, **471**, 18–27.
9 X. Wu, H. Chen, C. Wu, J. Wang, S. Zhang, J. Gao, H. Wang, T. Sun and Y. G. Yang, *Biomaterials*, 2018, **156**, 77–87.
10 M. C. P. Mendonca, A. Radaic, F. Garcia-Fossa, M. A. da Cruz-Hofling, M. A. R. Vinolo and M. B. de Jesus, *Drug Delivery Transl. Res.*, 2020, **10**, 34–42.
11 K. Tabatt, M. Sameti, C. Olbrich, R. H. Muller and C. M. Lehr, *Eur. J. Pharm. Biopharm.*, 2004, **57**, 155–162.
12 D. Pei and M. Buyanova, *Bioconjugate Chem.*, 2019, **30**, 273–283.
13 J. K. Laihia, J. P. Kallio, P. Taimen, H. Kujari, V. M. Kahari and L. Leino, *J. Invest. Dermatol.*, 2010, **130**, 2431–2439.
14 K. H. Bae, B. Shunmuganathan, L. Zhang, A. Lim, R. Gupta, Y. Wang, B. L. Chua, Y. Wang, Y. Gu, X. Qian, I. S. L. Tan, K. Purushotorman, P. A. MacAry, K. P. White and Y. Y. Yang, *npj Vaccines*, 2024, **9**, 43.
15 S. Sabnis, E. S. Kumarasinghe, T. Salerno, C. Mihai, T. Ketova, J. J. Senn, A. Lynn, A. Bulychev, I. McFadyen, J. Chan, O. Almarsson, M. G. Stanton and K. E. Benenato, *Mol. Ther.*, 2018, **26**, 1509–1519.
16 H. Akita, R. Ishiba, H. Hatakeyama, H. Tanaka, Y. Sato, K. Tange, M. Arai, K. Kubo and H. Harashima, *Adv. Healthcare Mater.*, 2013, **2**, 1120–1125.
17 X. Han, M.-G. Alameh, K. Butowska, J. J. Knox, K. Lundgreen, M. Ghattas, N. Gong, L. Xue, Y. Xu, M. Lavertu, P. Bates, J. Xu, G. Nie, Y. Zhong, D. Weissman and M. J. Mitchell, *Nat. Nanotechnol.*, 2023, **18**, 1105–1114.
18 I. Gonzalez-Dominguez, L. Cervera, F. Godia and M. Roldan, *J. Microsc.*, 2019, **273**, 53–64.
19 R. Kuai, D. Li, Y. E. Chen, J. J. Moon and A. Schwendeman, *ACS Nano*, 2016, **10**, 3015–3041.
20 L. Persegol, B. Verges, P. Gambert and L. Duvillard, *J. Lipid Res.*, 2007, **48**, 1396–1401.
21 W. Zhang, A. Pfeifle, C. Lansdell, G. Frahm, J. Cecillon, L. Tamming, C. Gravel, J. Gao, S. N. Thulasi Raman, L. Wang, S. Sauve, M. Rosu-Myles, X. Li and M. J. W. Johnston, *Vaccines*, 2023, **11**, 1580.
22 C. Bellefroid, C. Reusch, A. Lechanteur, B. Evrard, F. Debacq-Chainiaux, D. Mottet and G. Piel, *Int. J. Pharm.*, 2021, **593**, 120122.

23 W. Zhang, Y. Jiang, Y. He, H. Boucetta, J. Wu, Z. Chen and W. He, *Acta Pharm. Sin. B*, 2023, **13**, 4105–4126.
24 H. Farhood, N. Serbina and L. Huang, *Biochim. Biophys. Acta*, 1995, **1235**, 289–295.
25 P. C. Nguyen, M. T. T. Nguyen, S. Y. Ban, K. O. Choi, J. H. Park, P. L. Tran, J. W. Pyo, J. Kim and J. T. Park, *Food Chem.*, 2024, **437**, 137897.
26 M. Sune-Pou, S. Prieto-Sanchez, Y. El Yousfi, S. Boyero-Corral, A. Nardi-Ricart, I. Nofrerias-Roig, P. Perez-Lozano, E. Garcia-Montoya, M. Minarro-Carmona, J. R. Tico, J. M. Sune-Negre, C. Hernandez-Munain and C. Sune, *Int. J. Nanomed.*, 2018, **13**, 3223–3233.
27 A. Kontush, M. Lhomme and M. J. Chapman, *J. Lipid Res.*, 2013, **54**, 2950–2963.
28 C. Freitas and R. H. Muller, *Eur. J. Pharm. Biopharm.*, 1999, **47**, 125–132.
29 E. Tan, C. S. H. Chin, Z. F. S. Lim and S. K. Ng, *Front. Bioeng. Biotechnol.*, 2021, **9**, 796991.
30 J. Shi, M. W. Huang, Z. D. Lu, X. J. Du, S. Shen, C. F. Xu and J. Wang, *J. Controlled Release*, 2022, **345**, 494–511.
31 J. S. Suk, Q. Xu, N. Kim, J. Hanes and L. M. Ensign, *Adv. Drug Delivery Rev.*, 2016, **99**, 28–51.
32 P. Harvie, F. M. Wong and M. B. Bally, *J. Pharm. Sci.*, 2000, **89**, 652–663.
33 B. Tafech, M. R. Rokhforouz, J. Leung, M. M. Sung, P. J. Lin, D. D. Sin, D. Lauster, S. Block, B. S. Quon, Y. Tam, P. Cullis, J. J. Feng and S. Hedtrich, *Adv. Healthcare Mater.*, 2024, e2304525, DOI: **10.1002/adhm.202304525**.
34 J. M. Williford, M. M. Archang, I. Minn, Y. Ren, M. Wo, J. Vandermark, P. B. Fisher, M. G. Pomper and H. Q. Mao, *ACS Biomater. Sci. Eng.*, 2016, **2**, 567–578.
35 X. Hou, T. Zaks, R. Langer and Y. Dong, *Nat. Rev. Mater.*, 2021, **6**, 1078–1094.
36 P. Patel, N. M. Ibrahim and K. Cheng, *Trends Pharmacol. Sci.*, 2021, **42**, 448–460.
37 M. Schlich, R. Palomba, G. Costabile, S. Mizrahy, M. Pannuzzo, D. Peer and P. Decuzzi, *Bioeng. Transl. Med.*, 2021, **6**, e10213.
38 M. I. Harrell, B. M. Iritani and A. Ruddell, *J. Immunol. Methods*, 2008, **332**, 170–174.
39 J. N. Zuckerman, *BMJ*, 2000, **321**, 1237–1238.
40 N. Pardi, S. Tuyishime, H. Muramatsu, K. Kariko, B. L. Mui, Y. K. Tam, T. D. Madden, M. J. Hope and D. Weissman, *J. Controlled Release*, 2015, **217**, 345–351.
41 C. Efe, A. V. Kulkarni, B. Terziroli Beretta-Piccoli, B. Magro, A. Stattermayer, M. Cengiz, D. Clayton-Chubb, C. Lammert, C. Bernsmeier, O. Gul, F. H. la Tijera, M. Anders, E. Lytvyak, M. Akin, T. Purnak, R. Liberal, M. Peralta, B. Ebik, S. Duman, N. Demir, Y. Balaban, A. Urzua, F. Contreras, M. G. Venturelli, Y. Bilgic, A. Medina, M. Girala, F. Gunsar, M. C. Londono, T. Androutsakos, A. Kisch, A. Yurci, F. Guzelbulut, Y. F. Cagin, E. Avci, M. Akyildiz, E. K. Dindar-Demiray, M. Harputluoglu, R. Kumar, S. K. Satapathy, M. Mendizabal, M. Silva, S. Fagiuoli, S. K. Roberts, N. K. Soylu, R. Idilman, E. M. Yoshida, A. J. Montano-Loza, G. N. Dalekos, E. Ridruejo, T. D. Schiano and S. Wahlin, *Hepatology*, 2022, **76**, 1576–1586.
42 G. Schinas, E. Polyzou, V. Dimakopoulou, S. Tsoupra, C. Gogos and K. Akinosoglou, *World J. Virol.*, 2023, **12**, 100–108.
43 F. Ferraresso, A. W. Strilchuk, L. J. Juang, L. G. Poole, J. P. Luyendyk and C. J. Kastrup, *Mol. Pharmaceutics*, 2022, **19**, 2175–2182.
44 K. A. Whitehead, J. Matthews, P. H. Chang, F. Niroui, J. R. Dorkin, M. Severgnini and D. G. Anderson, *ACS Nano*, 2012, **6**, 6922–6929.
45 O. Escalona-Rayo, Y. Zeng, R. A. Knol, T. J. F. Kock, D. Aschmann, B. Slutter and A. Kros, *Biomed. Pharmacother.*, 2023, **165**, 115065.
46 K. Paunovska, C. D. Sago, C. M. Monaco, W. H. Hudson, M. G. Castro, T. G. Rudoltz, S. Kalathoor, D. A. Vanover, P. J. Santangelo, R. Ahmed, A. V. Bryksin and J. E. Dahlman, *Nano Lett.*, 2018, **18**, 2148–2157.
47 S. Ndeupen, Z. Qin, S. Jacobsen, A. Bouteau, H. Estanbouli and B. Z. Igyártó, *iScience*, 2021, **24**, 103479.
48 S. M. Moghimi and D. Simberg, *Mol. Ther.*, 2022, **30**, 2109–2110.
49 G. J. Leiros, A. G. Kusinsky, M. E. Balana and K. Hagelin, *J. Dermatol. Sci.*, 2017, **85**, 124–130.

